Real-time Quality Control for Offsite LGS Frames Manufacturing using Vision-Based Deep Learning

George Nader[1], Djamel Eddine Touil[1], Sai Praneeth Chandra Balla[1], Ahmed Bouferguene[2], Mohamed Al-Hussein[1] and Simaan AbouRizk[1]

[1]Department of Civil & Environmental Engineering, University of Alberta, Edmonton, Ab, T6G 2R3, Canada
[2]Campus Saint-Jean, University of Alberta, Edmonton, Ab, T6C 3N2, Canada

touil@ualberta.ca

Abstract -

Off-site light-gauge steel LGS frame manufacturing plays a key role in modern panelized construction due to its speed, precision, and reduced on-site labor. However, screw fastening defects remain a persistent issue that affects structural integrity, quality compliance, and production efficiency. This paper presents a real-time vision-based quality control framework integrated into a prototype LGS framing machine developed at the University of Alberta. The system equips the machine with visual perception using industrial cameras and a deep learning model to monitor screw fastening operations during production. A You Only Look Once (YOLO) v8-based computer vision system is used to detect screw conditions in real time and provide corrective feedback directly to the Programmable Logic Controller (PLC) via Modbus. Experimental results on five LGS wall panels (50 monitored fastening operations) demonstrate complete elimination of fastening defects under closed-loop control, with the defect rate reduced from 38% to 0%, supported by model precisions of 99.7% (LHS) and 99.1% (RHS). The proposed framework enhances assembly reliability while reducing operator dependency and rework, thereby supporting the transition toward autonomous, intelligent offsite construction systems.

Keywords -

Construction; Steel framing; Panelized; Quality Control; Computer vision

1 Introduction

Light-gauge steel LGS framing is widely used in off-site panelized and modular construction due to its structural efficiency, dimensional precision, and suitability for industrialised manufacturing. Its application in mid-rise, high-rise, and residential buildings has increased as off-site construction responds to labor shortages and the demand for higher productivity and quality consistency [1, 2]. Despite growing automation, screw fastening remains a critical and defect-prone operation. Defects such as misalignment, insufficient penetration, and incorrect angles directly affect structural performance and fabrication quality. These issues are mainly caused by material tolerances, actuator backlash, screw feeding inconsistencies, and dynamic disturbances during production.

Several studies have addressed automation and quality improvement in LGS manufacturing. Malik et al. [3] proposed automated toolpath generation for safe LGS panel fabrication, while Abushwereb et al. [4] introduced a manufacturing-centric Building Information Modelling (BIM) framework for light-frame construction. Martinez et al. further advanced the field by developing vision-based pre-inspection systems [5], automated manufacturability verification methods [6], and a cyber-physical framework for zero-defect manufacturing in LGS systems [7]. In addition, Martinez et al. [8] presented an online vision-based inspection system for detecting screw fastening defects in LGS frames. While these works significantly improved inspection and manufacturing reliability, most remain limited to pre- or post-process inspection and do not provide real-time corrective control embedded within machine actuation.

In parallel, deep learning and computer vision have demonstrated strong performance in steel structure and fastener inspection. Ameli et al. [9] applied YOLOv8 for steel bridge corrosion segmentation, while Chabi Adjobo et al. [10] proposed a YOLOv8-based object localization framework. Wu and Dong [11] enhanced YOLOv8 for improved real-time detection, and Terven et al. [12] reviewed YOLO architectures for engineering applications. Luo et al. [13] demonstrated YOLOv8-based industrial defect detection in automated production environments. These studies confirm the suitability of deep learning for high-speed structural inspection but highlight the lack of integration with real-time machine control in LGS manufacturing.

This paper addresses this gap by proposing a real-time vision-based quality control framework integrated into a prototype LGS framing machine. Two industrial cameras monitor the fastening zone, while a custom YOLOv8 model classifies screw conditions. The detected bounding box height is converted into a physical displacement using calibrated regression models and transmitted to the machine PLC via Modbus TCP/IP, enabling closed-loop, real-time correction of the screwdrivers during fastening. This integration supports the development of intelligent, self-correcting manufacturing systems for off-site steel construction.

The main contribution of this work is to directly link deep learning-based visual perception with PLC-level machine actuation for real-time error correction in LGS manufacturing. Unlike existing vision systems that operate in passive or post-process modes [5, 6, 7, 8], the proposed framework enables continuous monitoring and online process correction during screw fastening. Experimental results demonstrate that this integration significantly reduces fastening defects and improves overall manufacturing reliability in off-site LGS panel production.

2 Methodology

2.1 Architecture Overview

The proposed system is a real-time vision-based quality control framework, referred to hereafter as the Computer Vision System (CVS) [14], integrated into a LGS framing machine prototype for automated screw fastening [1]. The framework establishes a closed-loop interaction between perception, decision-making, and machine actuation to minimize fastening defects during production. The overall architecture is illustrated in Fig. 1 and organized into four functional blocks: Inputs, Main Process, Criteria, and Outputs.

The input layer consists of the BIM-based panel model, the trained YOLOv8n detection model, and the labelled image dataset. These inputs provide both the geometric context of the panel and the visual intelligence required for screw condition recognition.

The main process includes three modules. The Image Processing module performs real-time screw detection and classification using YOLOv8n on images captured by industrial cameras. The System Control module integrates these results with a Programmable Logic Controller (PLC) logic and BIM data to dynamically adjust screwdriver motion during fastening. The Human-Machine Interface (HMI) Visualization module displays real-time fastening status and defect information to support operator awareness and monitoring.

The Criteria block ensures that detected screw conditions comply with visual quality requirements and Canadian Standards Association (CSA) S136-07 S1-10 standards [15]. The output block represents the final results of the system, including real-time quality checking and adaptive control of the fastening operation. This architecture enables the transition from open-loop screw fastening to an intelligent cyber-physical manufacturing process.

2.2 Hardware Configuration

The LGS framing machine consists of two main fastening heads mounted on the left-hand side (LHS) and right-hand side (RHS), each equipped with a screwdriver driven along the Z-axis by a stepper motor. The machine operation is governed by a PLC that executes predefined sequences generated from a recipe (.RCP) file derived from the panel's digital model. However, conventional operation relies on pre-programmed motion commands without verification of actual screw position or quality during fastening.

To address this limitation, two Basler industrial cameras (aca640-90um) were installed facing the fastening zone to monitor the screw area in real time. Each camera captures video frames at 640×480 resolution and up to 90 frames per second, ensuring sufficient temporal and spatial resolution for detecting screw motion and position during high-speed operation. The cameras feature a global shutter, which eliminates motion blur caused by machine vibration during fastening, a critical property for reliable factory-floor deployment [16]. The cameras are rigidly co-mounted with the machine frame at approximately 80 cm from the fastening zone, minimizing relative displacement between the imaging plane and the screw-driving area during operation. The overall hardware and system configuration is illustrated in Fig. 2.

2.3 Model Training and Evaluation

The CVS processes real-time images and performs screw detection using the YOLOv8n (nano) object detection model, selected for its balance between inference speed and detection accuracy under the computational constraints of the industrial PC interfacing with the machine PLC.

Screws are classified into three categories: *ideal*, *keep-screwing*, and *defective*. The full dataset composition and split are summarized in Table 1 [14]. A total of 4,118 original images were collected for each side under varying fastening conditions. Four augmentation strategies were applied to improve model robustness: brightness adjustment (200 images), Gaussian noise (200 images), horizontal flipping (200 images), and negative samples (253 images), yielding a combined dataset of 4,971 images per side. Importantly, metal filings generated during the self-tapping process were present in all captured images and were included in training, providing implicit robustness to this common factory-floor contaminant. The dataset was split into training (4,146 images, 83%) and validation (825 images, 17%) sets. An additional independent holdout set of 350 unseen images per side was reserved exclusively for testing.

Table 1. Image dataset composition and allocation [14].

Image Type	Count
Original images	4,118
Brightened (augmented)	200
Noised (augmented)	200
Flipped horizontally	200
Negative samples	253
Total (Train + Val)	**4,971**
Training set (83%)	4,146
Validation set (17%)	825
Holdout test set	350

Per side (LHS and RHS trained separately).

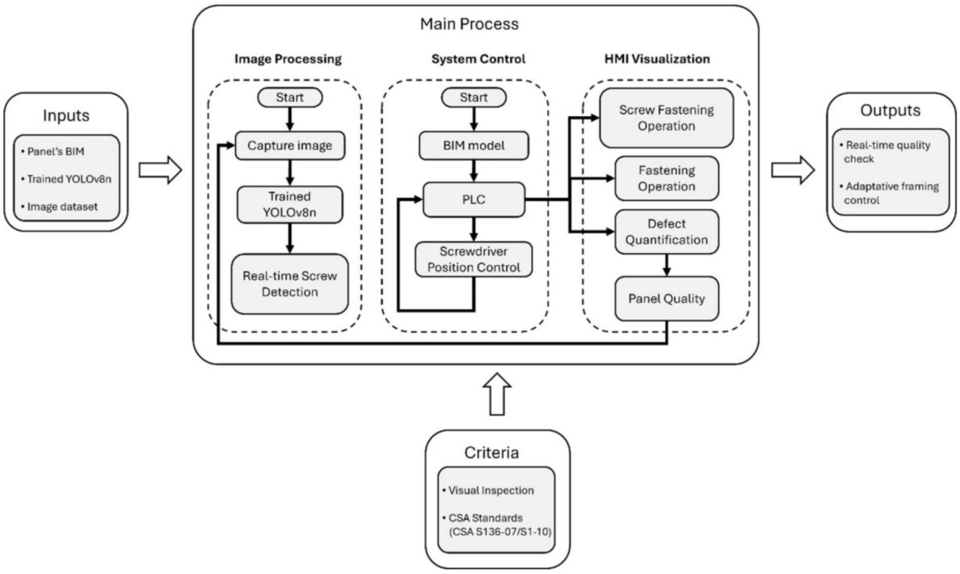

Figure 1. System Architecture Overview.

Dataset annotation was conducted using the Computer Vision Annotation Tool [17], as shown in Fig. 3. Separate models were trained for the left and right sides to account for camera perspective and machine geometric asymmetry, which is also reflected in the different calibration coefficients derived for each camera (Section 2.4).

2.4 Displacement Calibration

To convert visual information into actionable control input, the height of each detected bounding box is mapped to the physical screw penetration depth along the Z-axis. Since the cameras are rigidly mounted and the screw-driving zone forms a locally planar imaging region, the relationship between pixel height and real-world displacement can be approximated using a linear projection model.

Accordingly, the physical displacement d is expressed as a linear function of the detected bounding box height h_p (in pixels):

$$d = \alpha h_p + \beta, \tag{1}$$

where α and β are camera-specific calibration coefficients. To determine these coefficients for both the LHS and RHS cameras, a calibration experiment was conducted in which screws were driven to known depths while their corresponding pixel heights were recorded. The resulting pixel-to-millimetre relationships are illustrated in Fig. 4.

The parameters (α, β) for each camera were obtained using least-squares regression over M calibration samples $\{(h_{p,i}, d_i)\}$, by solving:

$$\min_{\alpha,\beta} \sum_{i=1}^{M} \left(d_i - (\alpha h_{p,i} + \beta)\right)^2 \tag{2}$$

The closed-form solutions are:

$$\alpha = \frac{\sum_{i=1}^{M}(h_{p,i} - \bar{h}_p)(d_i - \bar{d})}{\sum_{i=1}^{M}(h_{p,i} - \bar{h}_p)^2}, \qquad \beta = \bar{d} - \alpha \bar{h}_p \tag{3}$$

where $\bar{h}_p$ and $\bar{d}$ denote sample means. These coefficients were embedded into the control algorithm to provide real-time displacement estimates during fastening. The calibration is camera-position-specific; any repositioning of the cameras (e.g., following maintenance) requires re-running this procedure, which takes approximately 30 minutes per installation.

Based on the experimental calibration, the final regression models are:

$$\begin{bmatrix} d_{\text{LHS}} \\ d_{\text{RHS}} \end{bmatrix} = \underbrace{\begin{bmatrix} \alpha_{\text{LHS}} \\ \alpha_{\text{RHS}} \end{bmatrix}}_{\begin{bmatrix} 0.1364 \\ 0.1593 \end{bmatrix}} h_p + \underbrace{\begin{bmatrix} \beta_{\text{LHS}} \\ \beta_{\text{RHS}} \end{bmatrix}}_{\begin{bmatrix} 1.4580 \\ 0.2642 \end{bmatrix}} \tag{4}$$

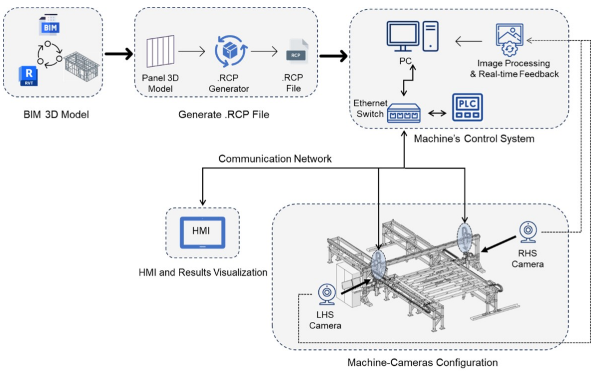

Figure 2. System Configuration using CVS Framework.

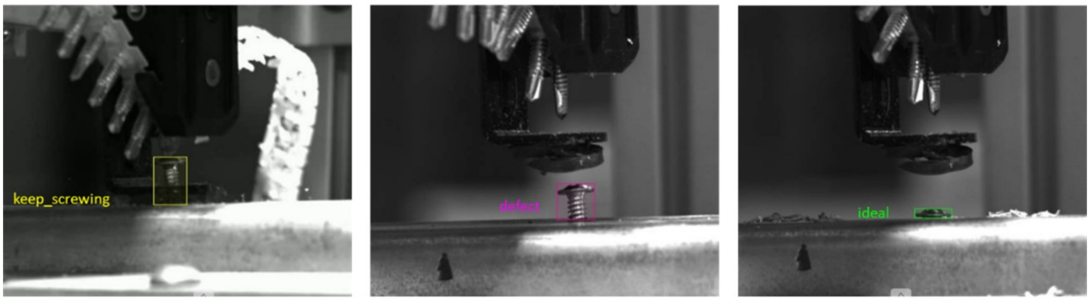

Figure 3. Image Annotation and Classification Examples for LHS and RHS Models.

2.5 Closed-Loop Control

Communication between the CVS and the PLC is implemented through the Modbus TCP/IP protocol, as illustrated in Fig. 5. The Python-based control script continuously processes camera frames, performs object detection, computes displacement values, and transfers them to predefined PLC registers. Four byte-type registers are used: two for the detected class (one per side) and two for the Z-axis displacement value (one per side). The class values transmitted are: 0 for *keep-screwing*, 1 for *defective*, and 2 for *ideal*.

A quality-check step was integrated into the PLC logic. During fastening, the PLC initiates screw insertion and waits for vision feedback. The system response for each detected class is as follows:

- *keep-screwing (0)*: Additional downward displacement is computed from the bounding box height via Eq. 1, converted to motor steps via Eq. 5, and applied to the actuator.

$$n_{steps} = 800 \times D_z \tag{5}$$

  where n_{steps} represents the real-time number of steps transferred from the PLC to the motor's driver, and D_z (equivalent to d from Eq. 1, in mm) is the displacement computed by the calibration model, with 1 mm corresponding to 800 motor steps.

- *ideal (2)*: The fastening operation stops and the screwdriver returns to the home position.

- *defective (1)*: The fastening operation stops immediately. The event is timestamped and logged to the production database, and the operator is alerted via an HMI notification specifying the defective screw position (LHS/RHS, stud number) for manual inspection.

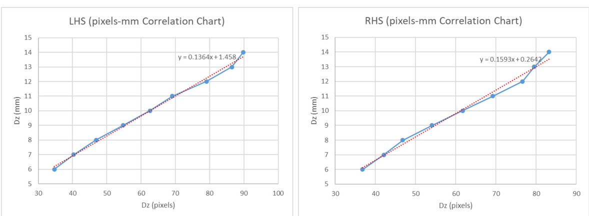

Figure 4. Pixels-mm correlation for LHS and RHS cameras.

The defect pathway does not attempt autonomous correction, as defects such as cross-threading or structural misalignment cannot be reliably resolved by additional downward driving. Flagging the event for operator intervention is the appropriate response to preserve structural integrity.

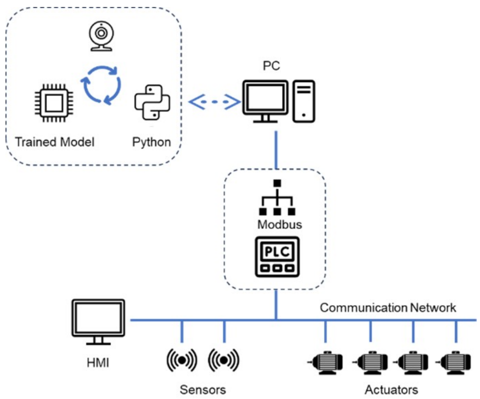

Figure 5. PLC-Python Communication Framework.

3 Results and Discussion

3.1 Experimental Setup

Five LGS wall panels were fabricated on the prototype machine at the University of Alberta, each comprising two tracks and five 14-gauge C-shaped studs fastened with 4.5 mm × 20 mm self-tapping screws. The CVS monitors the upper-side LHS and RHS screwdrivers, yielding 10 monitored operations per panel and 50 total. All panels were produced under identical conditions (same BIM model, RCP file, and stud spacing). Two scenarios were evaluated: (1) open-loop control using pre-programmed motion only, and (2) closed-loop CVS correction. Table 2 summarizes the real-time performance characteristics of the system.

The average end-to-end correction overhead is 0.66 s/screw, derived from the total increase in net ma-

Table 2. Real-time performance characterization [14].

Parameter	Value
Camera frame rate	90 fps
Camera resolution	640×480 pixels
Avg. end-to-end overhead	0.66 s/screw (ΔT_6 = 33 s / 50 screws)
Production speed control	Deterministic (PLC recipe)
T_5: Rework and transfer time (before / after CVS)	5.55 / 2.02 min (−64%)
T_6: Net running time (before / after CVS)	5.50 / 6.05 min (+0.55 min)
Total operating time	23.70 / 18.70 min (−5.0 min)

chine running time ($\Delta T_6 = 6.05-5.50 = 0.55$ min = 33 s across 50 monitored screws [14]). This value represents the average across all 50 operations, including screws already at the ideal position that incurred zero correction latency; the per-screw overhead for screws that required correction was therefore higher. Although T_6 increased slightly (+0.55 min total), this is offset by the 64% reduction in rework time (T_5), resulting in a net saving of 5.0 minutes in total operating time, confirming that CVS integration improves net throughput rather than reducing it.

As shown in Fig. 6, both YOLOv8n models achieved near-perfect performance: the LHS model reached a precision of 99.7%, recall of 100%, and mAP@0.5 of 99.5% (mAP@0.5–0.95: 95.0%), while the RHS model achieved a precision of 99.1%, recall of 100%, and mAP@0.5 of 99.1% (mAP@0.5–0.95: 95.0%). Precision was selected as the primary metric because a false positive (spurious actuator displacement) carries higher risk than a false negative in this PLC-control context.

The near-perfect precision on both sides (99.7% LHS, 99.1% RHS) confirms that displacement commands sent to the PLC are based on reliable detections, minimizing the risk of spurious actuator corrections. The perfect recall (100%) on both sides means no *keep-screwing* instance was missed. These results are consistent with the confusion matrices (Fig. 7), which show all diagonal entries at 1.0 with zero cross-class confusion, particularly between *keep-screwing* and *defective*, the most safety-critical boundary in this system.

Table 3. Design choice justification summary.

Decision	Chosen	Alternative	Rationale
Variants	YOLOv8n	YOLOv8s/m	Low task complexity; CPU real-time constraint
Scope	Separate LHS/RHS	Single unified	Geometric asymmetry; $\alpha_{\text{LHS}} \neq \alpha_{\text{RHS}}$
Metrics	Precision	Recall/mAP	False positive cost > false negative in PLC control

Table 3 summarizes the three principal design decisions. YOLOv8n was preferred over larger variants as the three-class detection task does not require higher model complexity, and the nano variant meets the real-time constraint of the industrial PC. Separate LHS and RHS models were trained rather than a single unified model due to the machine geometric asymmetry, confirmed by the differing calibration slopes ($\alpha_{\text{LHS}} = 0.1364$ vs. $\alpha_{\text{RHS}} = 0.1593$). Precision was selected as the primary evaluation metric because a false positive – incorrectly triggering additional actuator displacement – carries higher risk than a false negative in this PLC-control context.

The live detection results are shown in Fig. 8. The system tracked screw conditions reliably during high-speed fastening despite machine vibration and metal filing debris.

Table 4 reports the per-panel defect results. Open-loop operation produced 19 defects across 50 operations (mean: 38.0%, SD: 20.5%), confirming the inherent instability of fixed-profile fastening. Closed-loop CVS activation eliminated all defects across all five panels (0/50). The 5-out-of-5 zero-defect consistency confirms the repeatability of the correction mechanism. Model generalizability is further supported by consistent detection performance on an independent holdout set of 350 unseen images per side [14], with validation set precision of 99.7% (LHS) and 99.1% (RHS).

The high SD of 20.5% in the open-loop scenario (panel rates ranging from 20% to 60%) reveals that the defect problem reflects genuine mechanical variability – actuator backlash, material tolerances, and stud positioning errors – that a static pre-programmed profile fundamentally cannot address. The CVS resolves this by measuring and correcting each screw independently in real time, decoupling quality from panel-to-panel mechanical variation.

Table 4. Per-panel defect results: open-loop (without CVS) vs. closed-loop (with CVS) [14].

Panel	Without CVS		With CVS	
	Defects	Rate (%)	Defects	Rate (%)
Panel 1	2	20	0	0
Panel 2	3	30	0	0
Panel 3	2	20	0	0
Panel 4	6	60	0	0
Panel 5	6	60	0	0
Total	**19/50**	**38 avg**	**0/50**	**0**

LHS: 7 defects; RHS: 12 defects (open-loop). Mean and SD computed from per-panel rates.

3.2 Overall Equipment Effectiveness Analysis

To further quantify the impact of CVS integration on machine performance, the Overall Equipment Effectiveness (OEE) framework was applied following the methodology detailed in [14]. Timers embedded in the PLC code record the duration of each production phase. Table 5 defines all timer variables used in the OEE equations.

The ideal cycle time per panel is computed as [14]:

$$t_{\text{ideal}} = \frac{T_6}{N} + N_{\text{studs}} \times 10 + 15 \quad \text{[s/panel]} \tag{6}$$

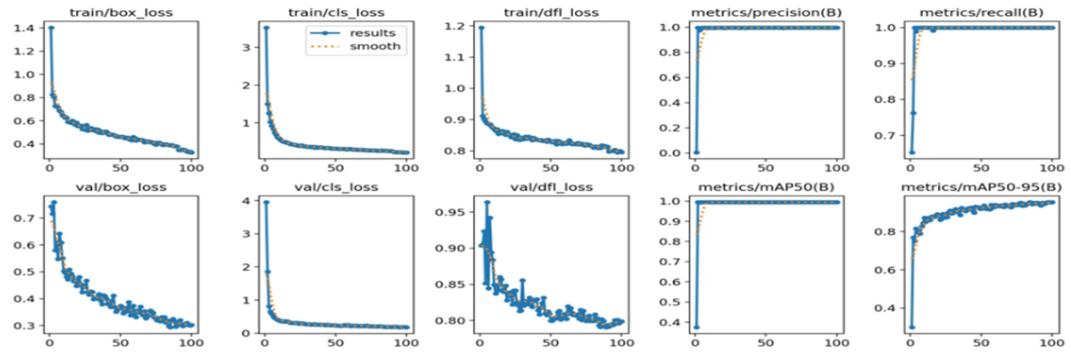

(a) LHS model training results

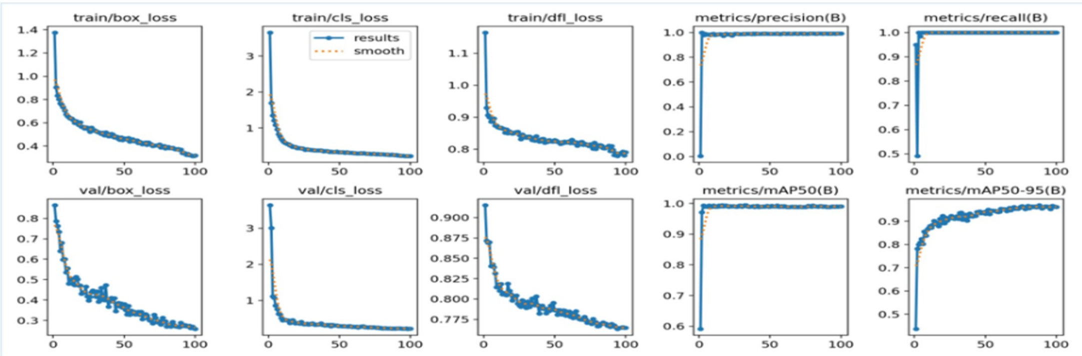

(b) RHS model training results

Figure 6. (a) LHS model training results, (b) RHS model training results.

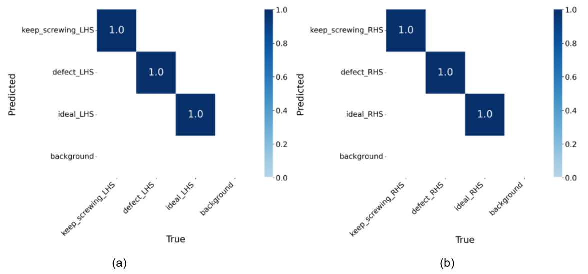

Figure 7. Confusion Matrices Normalized for Image Classification of (a) LHS and (b) RHS Models.

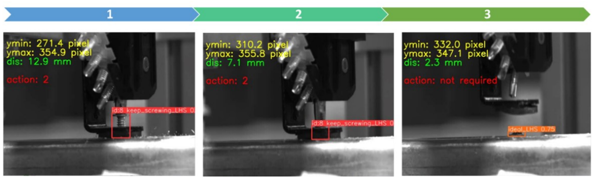

Figure 8. Experiment Implementation Using Proposed CVS Framework.

where all variables are defined in Table 5. Note that T_6 must be converted to seconds when substituting into Eq. 6. OEE is computed as the product of three indicators [14]:

$$\mathrm{OEE}\% = A\% \times P\% \times Q\% \tag{7}$$

Table 5. PLC timer and variable definitions for OEE computation [14].

Symbol	Definition
T_1	Total panel cycle time (machine production time, excluding rework)
T_2	Total track loading time
T_s	Total stud loading time
T_4	Machine calibration time (downtime)
T_5	Rework and panel transfer time
T_6	Net machine running time, $T_6 = T_1 - (T_s + T_2)$
N_{out}	Number of panels produced (5 in this experiment)
N_{studs}	Number of studs per panel (5 in this experiment)
t_{ideal}	Ideal cycle time per panel (no defects, no waiting)
N_{ops}	Total monitored fastening operations (50)
N_{def}	Total number of detected defects

where Availability ($A\%$), Performance ($P\%$), and Quality ($Q\%$) are defined as:

$$A\% = \frac{T_1 + T_5}{T_1 + T_4 + T_5} \times 100$$

$$P\% = \frac{t_{\mathrm{ideal}} \times N_{\mathrm{out}}}{T_1 + T_5} \times 100 \tag{8}$$

$$Q\% = \frac{N_{\mathrm{ops}} - N_{\mathrm{def}}}{N_{\mathrm{ops}}} \times 100$$

where all symbols are as defined in Table 5.

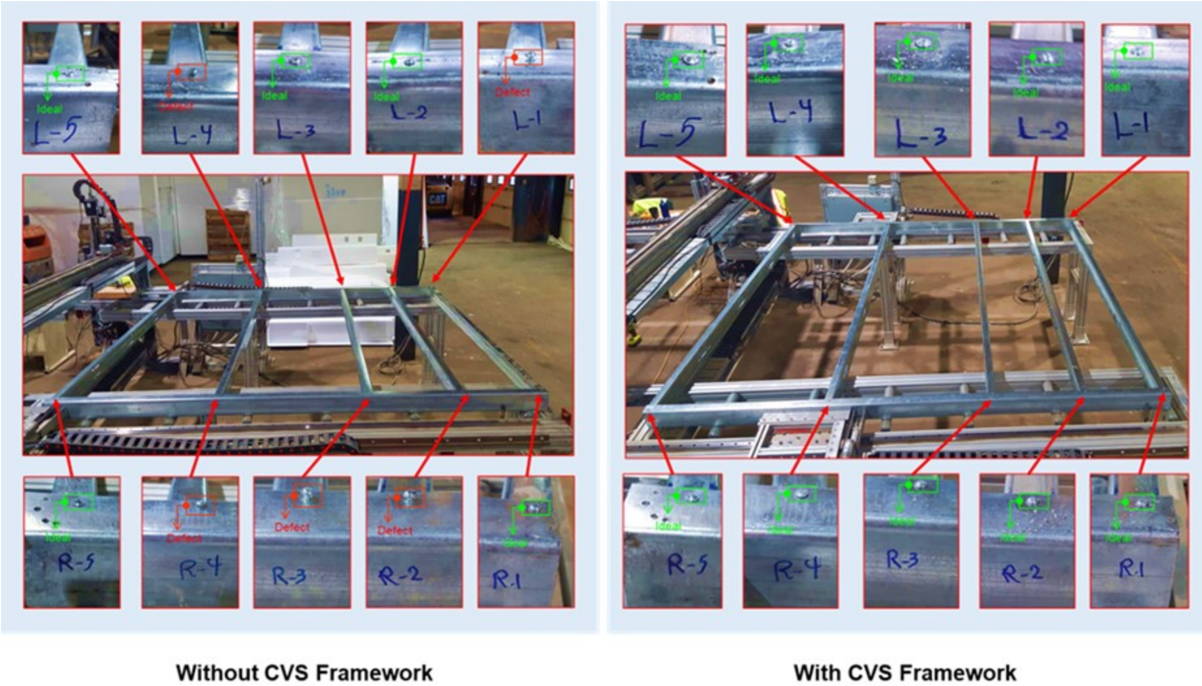

Figure 9. Experimental Comparison: Without CVS (left) vs. With CVS (right).

Table 6 summarizes the OEE metrics before and after CVS integration. CVS integration drove $Q\%$ from 62% to 100% by eliminating all 19 defects, and improved $P\%$ from 46.0% to 61.3% through reduction of rework-induced idle time. Rework and transfer time (T_5) decreased by 64% (5.55 to 2.02 min), directly reflecting the elimination of post-fastening repair. Overall OEE more than doubled from 27.9% to 59.5%.

Table 6. OEE metrics before and after CVS integration [14].

Metric	Without CVS	With CVS	Change
$A\%$	97.7%	97.1%	−0.6 pp
$P\%$	46.0%	61.3%	+15.3 pp
$Q\%$	62.0%	100.0%	+38.0 pp
OEE%	27.9%	59.5%	+31.6 pp
T_5 (min)	5.55	2.02	−64%

pp = percentage points.

The OEE results reveal distinct contributions of CVS to each indicator. $Q\%$ improved from 62% to 100% purely through defect elimination, a direct consequence of closed-loop correction. $P\%$ improved from 46.0% to 61.3% because reducing T_5 shrinks the gap between actual and ideal cycle time. The slight decrease in $A\%$ (97.7% to 97.1%) is expected: reducing T_5 mathematically lowers the loading time denominator in Eq. 8, a known artefact of the OEE formulation when rework time is part of operating time [14]. Collectively, the dominant gains in $P\%$ and $Q\%$ drove OEE from 27.9% to 59.5%, more than doubling overall machine effectiveness. The visual comparison in Fig. 9 further illustrates the outcome: without CVS, multiple screw positions show misalignment or under-driving; with CVS, all positions reach the ideal condition.

These findings extend prior research by embedding the vision model directly into the machine control loop rather than using it as a passive inspection tool, representing a practical step toward intelligent, self-correcting manufacturing for civil and construction engineering applications.

4 Conclusion

Unlike existing vision-based inspection systems that operate in passive or post-process modes, this study presented a real-time vision-based quality control framework integrated into a prototype Light Gauge Steel framing machine. By combining YOLOv8-based screw detection with PLC-level actuation through a closed-loop quality-check step, the system dynamically corrects screw penetration during fastening. Experimental results on five LGS wall panels (50 monitored fastening operations) demonstrated complete elimination of fastening defects: the defect rate dropped from 38% (19/50) to 0%, model precision reached 99.7% (LHS) and 99.1% (RHS), OEE improved from 27.9% to 59.5%, and rework time was reduced by 64%. These outcomes confirm that embedding deep learning perception directly into machine control significantly enhances fastening accuracy and supports higher-quality LGS panel production. The proposed framework represents a practical advancement toward intelligent, self-correcting manufacturing systems tailored for offsite and industrialized construction environments.

5 Limitations and Future Work

The experiments were conducted on five panels under controlled laboratory conditions using a single LGS profile and screw type; changes in steel gauge, stud geometry, or screw type require model retraining and recalibration, as does camera repositioning (~30 min). Furthermore, the CVS relies exclusively on visual information to infer screw quality. While effective for detecting penetration depth defects, vision-based inspection cannot capture all quality-relevant parameters of a fastening operation, such as torque, thread engagement, or internal structural integrity. Future work will explore multi-sensor fusion combining vision with force and torque feedback to provide more comprehensive quality assurance within the existing Modbus TCP/IP framework. Further extensions include validation under variable lighting and production speeds, formal ablation of model architecture choices, integration with plant-level SCADA and digital twin frameworks, and IP65- rated camera enclosures for full industrial deployment.

References

[1] Pablo Martinez, Mohamed Al-Hussein, and Rafiq Ahmad. Intelligent vision-based online inspection system of screw-fastening operations in light-gauge steel frame manufacturing. *The International Journal of Advanced Manufacturing Technology*, 109(3):645–657, 2020.

[2] Sang Jun Ahn, SangUk Han, Mohammed Sadiq Altaf, and Mohamed Al-Hussein. Integrating off-site and on-site panelized construction schedules using fleet dispatching. *Automation in Construction*, 137:104201, 2022.

[3] Nabeel Malik, Rafiq Ahmad, and Mohamed Al-Hussein. Generation of safe tool-paths for automatic manufacturing of light gauge steel panels in residential construction. *Automation in Construction*, 98:46–60, 2019.

[4] Mahmud Abushwereb, Hexu Liu, and Mohamed Al-Hussein. A knowledge-based approach towards automated manufacturing-centric bim: wood frame design and modelling for light-frame buildings. *Modular and Offsite Construction (MOC) Summit Proceedings*, pages 100–107, 2019.

[5] Pablo Martinez, Rafiq Ahmad, and Mohamed Al-Hussein. A vision-based system for pre-inspection of steel frame manufacturing. *Automation in Construction*, 97:151–163, 2019.

[6] Shi An, Pablo Martinez, Mohamed Al-Hussein, and Rafiq Ahmad. Automated verification of 3d manufacturability for steel frame assemblies. *Automation in Construction*, 118:103287, 2020.

[7] Pablo Martinez, Mohamed Al-Hussein, and Rafiq Ahmad. A cyber-physical system approach to zero-defect manufacturing in light-gauge steel frame assemblies. *Procedia Computer Science*, 200:924–933, 2022.

[8] Pablo Martinez, Mohamed Al-Hussein, and Rafiq Ahmad. Intelligent vision-based online inspection system of screw-fastening operations in light-gauge steel frame manufacturing. *The International Journal of Advanced Manufacturing Technology*, 109(3):645–657, 2020.

[9] Zahra Ameli, Shabnam Jafarpoor Nesheli, and Eric N Landis. Deep learning-based steel bridge corrosion segmentation and condition rating using mask rcnn and yolov8. *Infrastructures*, 9(1):3, 2023.

[10] Esther Chabi Adjobo, Amadou Tidjani Sanda Mahama, Pierre Gouton, and Joël Tossa. Automatic localization of five relevant dermoscopic structures based on yolov8 for diagnosis improvement. *Journal of Imaging*, 9(7):148, 2023.

[11] Tianyong Wu and Youkou Dong. Yolo-se: Improved yolov8 for remote sensing object detection and recognition. *Applied Sciences*, 13(24):12977, 2023.

[12] Juan Terven, Diana-Margarita Córdova-Esparza, and Julio-Alejandro Romero-González. A comprehensive review of yolo architectures in computer vision: From yolov1 to yolov8 and yolo-nas. *Machine Learning and Knowledge Extraction*, 5(4): 1680–1716, 2023.

[13] Bingxin Luo, Ziming Kou, Cong Han, and Juan Wu. A "hardware-friendly" foreign object identification method for belt conveyors based on improved yolov8. *Applied Sciences*, 13(20):11464, 2023.

[14] George Nader. Real-time quality control for offsite LGS frame manufacturing using vision-based deep learning. MSc thesis, University of Alberta, 2024.

[15] Pablo Martinez. Automatic intelligent inspection systems for quality control: A case of defects in light-gauge steel frame assembly manufacturing. 2020.

[16] Basler AG. *Basler ace USB3 Area Scan Camera – Product Data Sheet: Model acA640-90um*. Basler AG, 2022. URL `https://www.baslerweb.com/en/products/cameras/area-scan-cameras/ace/aca640-90um/`. Sensor: Sony ICX424, CCD global shutter, 90 fps at 659×494 resolution.

[17] CVAT.ai Corporation. Computer vision annotation tool (cvat). URL `https://cvat.ai/`.